Developmental Biology 404 (2015) 21–34

Contents lists available at ScienceDirect

Developmental Biology

journal homepage: www.elsevier.com/locate/developmentalbiology

Identification of HECT E3 ubiquitin ligase family genes involved in stem cell regulation and regeneration in planarians

Jordana M. Henderson [a], Sean V. Nisperos [a], Joi Weeks [a], Mahjoobah Ghulam [a], Ignacio Marín [b], Ricardo M. Zayas [a,*]

[a] Department of Biology, San Diego State University, San Diego, CA 92182-4614, USA
[b] Instituto de Biomedicina de Valencia, Consejo Superior de Investigaciones Científicas (IBV-CSIC), Valencia, Spain

ARTICLE INFO

Article history:
Received 28 May 2014
Received in revised form
14 March 2015
Accepted 27 April 2015
Available online 6 May 2015

Keywords:
HECT
Planarian
Stem cells
HUWE1
TRIP12
WWP1

ABSTRACT

E3 ubiquitin ligases constitute a large family of enzymes that modify specific proteins by covalently attaching ubiquitin polypeptides. This post-translational modification can serve to regulate protein function or longevity. In spite of their importance in cell physiology, the biological roles of most ubiquitin ligases remain poorly understood. Here, we analyzed the function of the HECT domain family of E3 ubiquitin ligases in stem cell biology and tissue regeneration in planarians. Using bioinformatic searches, we identified 17 HECT E3 genes that are expressed in the *Schmidtea mediterranea* genome. Whole-mount *in situ* hybridization experiments showed that HECT genes were expressed in diverse tissues and most were expressed in the stem cell population (neoblasts) or in their progeny. To investigate the function of all HECT E3 ligases, we inhibited their expression using RNA interference (RNAi) and determined that orthologs of *huwe1*, *wwp1*, and *trip12* had roles in tissue regeneration. We show that *huwe1* RNAi knockdown led to a significant expansion of the neoblast population and death by lysis. Further, our experiments showed that *wwp1* was necessary for both neoblast and intestinal tissue homeostasis as well as uncovered an unexpected role of *trip12* in posterior tissue specification. Taken together, our data provide insights into the roles of HECT E3 ligases in tissue regeneration and demonstrate that planarians will be a useful model to evaluate the functions of E3 ubiquitin ligases in stem cell regulation.

Introducton

Planarians are capable of regenerating complete worms from very small body fragments; their prodigious regenerative capacity is conferred by a population of adult stem cells, called neoblasts, that can replace all cells lost during normal cellular turnover or tissue loss. Following injury, planarian stem cells proliferate and give rise to the regeneration blastema and differentiate into the missing tissues. Thus, planarians have emerged as an important model system to investigate molecular mechanisms underpinning stem cell biology and organ regeneration. Studies using the model planarian *Schmidtea mediterranea* have led to experimental dissection of processes such as tissue regeneration (Reddien et al., 2005), tissue patterning (Adell et al., 2010; Forsthoefel and Newmark, 2009; Forsthoefel et al., 2011; Reddien, 2011), wound response and regeneration initiation (Petersen and Reddien, 2009; Wenemoser et al., 2012), and the mechanisms underlying inductive germ cell specification (Newmark et al., 2008; Wang et al., 2010). The ability to isolate stem cell, progenitor cell, and differentiated cell populations using flow cytometry has facilitated whole-genome transcriptome analyses that revealed a high degree of conservation of pluripotency determinants between mammalian and planarian stem cells (Labbé et al., 2012; Önal et al., 2012; Resch et al., 2012).

By contrast, little is known about how regulation of the proteome contributes to regenerative events. Two-dimensional gel electrophoresis combined with mass spectrometry has been used to identify proteins enriched in the neoblasts (Férnandez-Taboada et al., 2011); and, most recently, SILAC proteomics were successfully used to identify stem cell-specific proteins in planarians (Boser et al., 2013). However, no studies have been aimed at elucidating how dynamic regulation of the proteome underscores planarian regeneration.

As a first step in addressing the role of protein regulation in tissue renewal, we sought to characterize the role of E3 ubiquitin ligases. Ubiquitylation is the transfer of free ubiquitin onto a protein substrate through a cascade of E1, E2, and E3 ubiquitin-associated enzymes (Ardley and Robinson, 2005; Ciechanover et al., 1984; Scheffner et al., 1995). E3 function regulates protein degradation,

* Correspondence to: Department of Biology, San Diego State University, 5500 Campanile Dr. San Diego, CA 92182-4614, USA. Fax: +1 619 594 5676.
E-mail address: rzayas@mail.sdsu.edu (R.M. Zayas).

http://dx.doi.org/10.1016/j.ydbio.2015.04.021
0012-1606/

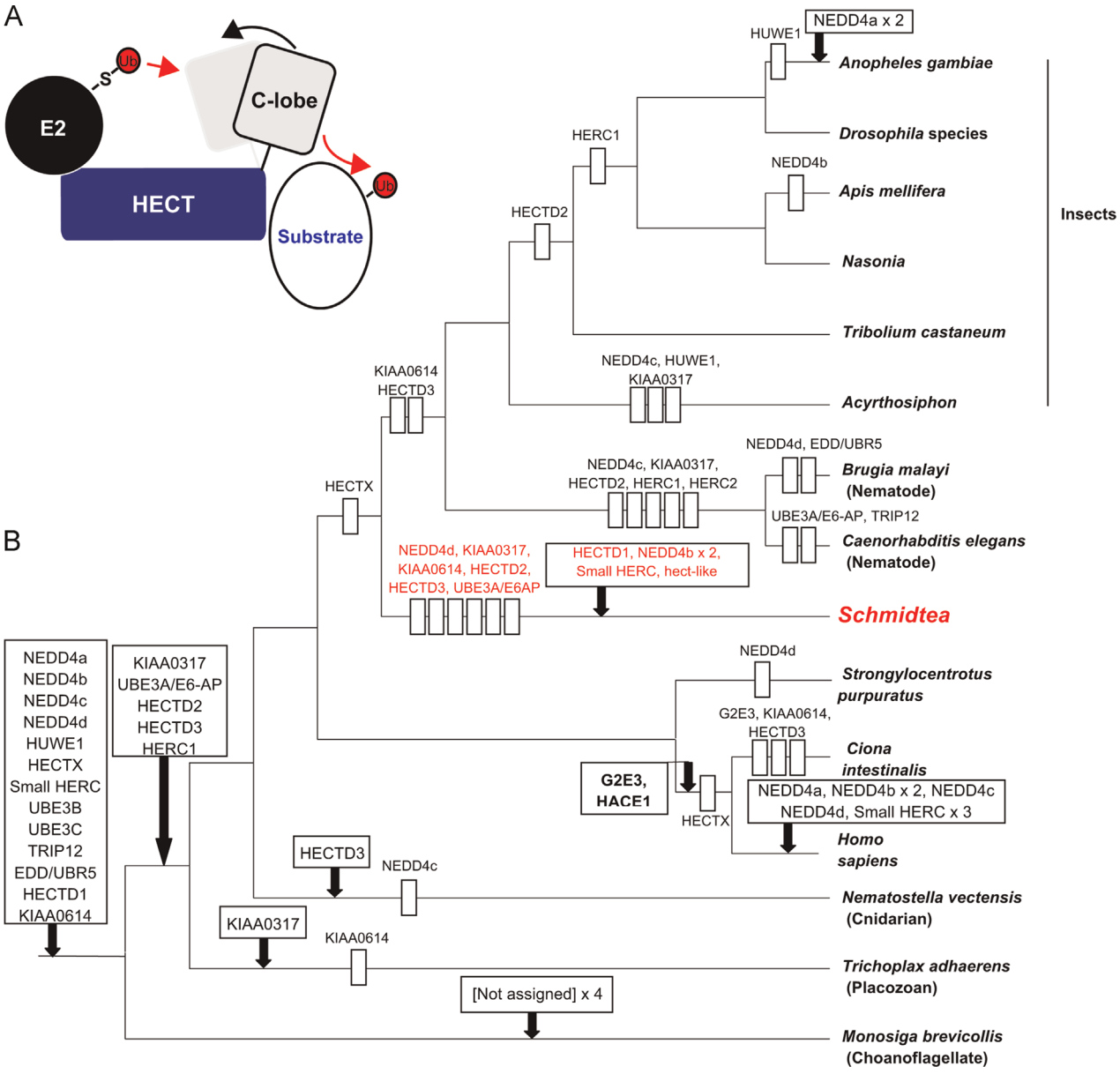

Fig. 1. Phylogenetic relationships of HECT E3 ubiquitin ligase across metazoans. (A) Illustration of HECT E3 domain structure and ubiquitylation of protein substrates. Ubiquitylation involves sequential activity of three enzymes: E1 activating enzymes (not illustrated) bind ubiquitin (Ub) *via* a thioester bond (–S–). Ubiquitin is transferred from E1 to an E2 conjugating enzyme. HECT E3s bind substrates directly. Ubiquitin is first transferred from E3 enzymes to a C-lobe with a flexible hinge loop and then to the substrate (Metzger et al., 2012). (B) Most parsimonious phylogenetic tree reconstruction of HECT-domain E3 ligase gene relationships in animals. The *Schmidtea mediterranea* genes are highlighted in red. Arrows indicate the emergence of new genes and rectangles indicate gene losses. Data from Marín (2010) and this study.

apoptosis, signaling, protein trafficking, and transcription (Hershko and Ciechanover, 1998; Jacobson et al., 2009; Komander, 2009). E3 ubiquitin ligases are grouped into two major classes: HECT (*H*omologous to the *E*6-AP *C*arboxyl *T*erminus)-domain and RING (*R*eally *I*nteresting *N*ew *G*ene)-finger E3 ligases (Ardley and Robinson, 2005; Kipreos, 2005; Metzger et al., 2012). HECT E3 ligases directly bind their targets and catalyze ubiquitin transfer (Huibregtse et al., 1995; Metzger et al., 2012) (Fig. 1A). HECT domains were discovered nearly 20 years ago as a result of their similarity to E6 proteins of human papilloma virus (Huibregtse et al., 1995). Several HECT E3s have been implicated in both normal development and the emergence of different types of cancer such as pancreatic (*smurf1*), breast (*huwe1* and *wwp1*), and ovarian (*ubr5*) (Bernassola et al., 2008; Scheffner and Staub, 2007). Therefore, understanding the normal biological roles and specific targets in developmental processes should help elucidate how misregulation of HECT E3s can lead to diseases and reveal potential therapeutic targets.

Using the *S. mediterranea* genome, we identified 17 HECT-domain genes, obtained the sequences, and determined their tissue specific patterns of expression by whole mount *in situ* hybridization (WISH), which showed that 11 of these genes are expressed in the neoblasts or in their progeny. RNA interference (RNAi) experiments revealed that three HECT E3s, *trip12*, *huwe1*, and *wwp1*, were required for tissue regeneration, and uncovered a surprising role for *trip12* in establishing and maintaining posterior polarity. RNAi knockdown of *huwe1* or *wwp1* resulted in neoblast regulation defects, including a strong expansion of the neoblast population in *huwe1* RNAi planarians and a significant loss of neoblasts following *wwp1* knockdown. In addition, we found that *wwp1* was strongly expressed in the planarian intestine and its expression was required for maintenance of this organ. Our study identifies specific biological roles for a subset of HECT-domain

ubiquitin ligases in planarian biology. Furthermore, our data demonstrate that knockdown of neoblast-expressed E3 ubiquitin ligases can result in strong phenotypes that could serve as biological readouts for downstream identification of E3 specific protein targets required for stem cell regulation and tissue regeneration..

Materials and methods

Planarian care

A clonal line of asexual *S. mediterranea* (CIW4) were maintained in 1X Instant Ocean Salts (0.83 mM $MgSO_4$, 0.9 mM $CaCl_2$, 0.04 mM $KHCO_3$, 0.9 mM $NaHCO_3$, and 0.21 g/L Instant Ocean Aquarium Salt diluted in ultra-pure water) at 20 °C. Animals were starved for 1 week and those ranging between 2–5 mm in length were selected for experimentation.

Gene identification and phylogenetic analysis

Using TBLASTN searches against the nr, est, htgs, gss, wgs, and tsa databases available at the National Center for Biotechnology Information (NCBI; http://www.ncbi.nlm.nih.gov/) 17 HECT-domain containing protein coding sequences and one pseudogene were identified in *S. mediterranea*. ClustalX 2.0.12 (Larkin et al., 2007) was used to align the 17*S. mediterranea* gene sequences with those in a HECT domain database containing 877 sequences (Marín, 2010). Manual corrections were made to the alignments using GeneDoc 2.7 (Nicholas and Nicholas, 1997). Phylogenetic analyses were performed using Neighbor-Joining (NJ), Maximum-Parsimony (MP), and Maximum-Likelihood (ML) as previously described (Marín, 2010, 2013). NJ and ML trees were obtained using MEGA 5.2 (Tamura et al., 2011), and maximum-parsimony (MP) trees were obtained using PAUP* 4.0, beta 10 version (Swofford, 2003). For NJ, Kimura's correction was used, and sites with gaps were treated with the pairwise deletion option. Parameters for MP analyses of full-length sequences were as follows: (1) all sites were included, gaps treated as unknown characters; (2) randomly generated trees used as seeds; (3) maximum number of trees saved equal to 100; and (4) heuristic search using the subtree-pruning-regrafting (SPR) algorithm with default parameters. For ML analyses, the BioNJ tree was taken as starting point for the iterative searches, using the Jones–Taylor–Thornton (JTT) model of amino acidic substitutions. According to the ML model comparison analyses available in MEGA 5.2, the best fit was obtained with the JJT model, a discrete gamma (G) distribution with five categories of sites to account for heterogeneity in evolutionary rates, and the empirical amino acid frequencies (F) of the dataset. ML tree topologies were explored using the default, fast SPR algorithm. Bootstrap tests were performed to establish the reliability of the final dendrograms obtained in the NJ, MP, and ML analyses. A total of 1000 replicates were generated for NJ analyses, and 100 replicates were made for the MP and ML analyses, which are much more computer-intensive.

Cloning and whole mount in situ hybridization

Partial sequences of the identified HECT genes were obtained from a cDNA collection (Zayas et al., 2005) or cloned into pJC53.2 (Collins et al., 2010), using gene specific primers (Table S1). Single-stranded, antisense RNA probes were synthesized and hybridized to formaldehyde-fixed animals as previously described (Pearson et al., 2009) in an Intavis InsituPro VS liquid handling robot. Samples were incubated with anti-digoxigenin-AP antibody (Roche, 1:2000) and developed with NBT/BCIP or Fast Blue as previously described (Cowles et al., 2013) or incubated with anti-FITC-POD antibody (Roche, 1:300) and detected using Tyramide Signal Amplification (TSA) for double fluorescence. Animals treated with γ-irradiation were exposed to 100 Gy in a JL Shepherd Mark I Cesium-137 irradiator.

RNA interference

Double-stranded RNA (dsRNA) expression was induced by IPTG in HT115(DE3) cells containing gene constructs in pJC53.2. Animals were fed bacterially expressed dsRNA 6–20 times, as previously described (Gurley et al., 2008; Sánchez Alvarado and Newmark, 1999). One day after the final feeding, animals were amputated anterior or posterior to the pharynx and allowed to regenerate for 7–10 days.

Immunohistochemistry

Planarians were killed in ice cold 2% hydrochloric acid for 5 min and fixed in Carnoy's solution (6:3:1 ethanol, chloroform, and glacial acetic acid) for 2 h at 4 °C then incubated in 100% methanol for 1 h at 4 °C and bleached overnight in 6% hydrogen peroxide diluted in methanol. Animals were washed out of methanol into PBSTx and blocked in 1% BSA diluted in PBSTx for 2 h prior to anti-phosphohistone-H3 (Ser10) (1:1000, Cell Signaling) (Hendzel et al., 1997; Hubert et al., 2013) staining. For anti-3G9 staining, animals were processed as previously described (Forsthoefel et al., 2012). All antibodies were detected using a TSA protocol as described previously (King and Newmark, 2013). Briefly, animals were incubated for 10 min in a borate buffer before TSA reaction in a borate-FITC reaction buffer for 15–30 min then washed out in PBSTx. Borate buffer contained 0.1 M borate pH 8.5 and 0.1% Tween-20 diluted in ultrapure water. Borate-FITC reaction buffer contained 0.1 M borate pH 8.5, 0.1% Tween-20, 2% dextran sulfate, 0.003% hydrogen peroxide, and 4 μg FITC-tyramide diluted in ultrapure water (Lauter et al., 2011).

BrdU labeling

Specimens were soaked in 5-bromo-2-deoxyuridine (BrdU) for a 1 h pulse and fixed after a 2 h chase as previously described (Cowles et al., 2012).

TUNEL staining

Terminal deoxynucleotidyl transferase-mediated deoxyuridine-triphosphate nick end-labeling (TUNEL) staining was used to analyze levels of apoptosis. For TUNEL assays, animals were incubated in 10% NAC for 5 min and fixed in 4% formaldehyde plus 1% SDS for 20 min. Samples were then bleached and stained with the Apoptag Kit (Millipore) as previously described (Pellettieri et al., 2010).

Flow cytometry analysis

Flow cytometry was performed on papain-dissociated animals stained with Hoechst 33342 dye (Thermo Scientific) (Romero et al., 2012). For standardization, 10,000 data events per population of interest were acquired on a BD FACSAria flow cytometer. Hoescht-stained cells were excited using a 375 nm near UV laser. A 595-long pass dichroic mirror followed by a 605/40 band-pass filter was used for red emission, and a 450/20 band-pass filter was used for blue emission. Data were analyzed with BD FACSDiva. An additional control group was exposed to 100 Gy γ-irradiation 3 or 4 days prior to dissociation using a JL Shepherd Mark I Cesium-137 irradiator to set the gates for quantifying stem cell (irradiation-sensitive population 1; X1), stem cell progeny (irradiation-

Table 1
HECT-domain E3 ubiquitin ligase class subfamilies present in *Schmidtea mediterranea*.

HECT Subfamily	*S. mediterranea* gene name	Acc. no.	Presence in other flatworm species[a]	Notes
NEDD4a	***Smed-nedd4***	GAKN01004003.1	*Echinococcus* (1), *Taenia* (1), *Hymenolepis* (1), *Schistosoma* (1), *Procotyla* (2), *Dugesia* (0)	Ortholog of mammalian NEDD4, NEDD4L
NEDD4b	***Smed-wwp1-like-1***	GAKN01013806.1	*Echinococcus* (1), *Taenia* (2), *Hymenolepis* (1), *Schistosoma* (2), *Procotyla* (3), *Dugesia* (2–3)	Orthologs of the mammalian genes WWP1, WWP2 and ITCH. The *Schmidtea* genes are recent duplicates, present only in closely related species. A potential pseudogene (sequence anomalous, with stop codons) also found: AAWT01001557.1
	Smed-wwp1-like-2	GAKN01002039.1		
	Smed-wwp1-like-3	GAKN01011959.1		
NEDD4c	***Smed-smurf***	GAKN01002365.1	*Echinococcus* (0), *Taenia* (0), *Hymenolepis* (0), *Schistosoma* (0), *Procotyla* (1), *Dugesia* (1)	Ortholog of mammalian SMURF1, SMURF2
NEDD4d		Not found	Not found	Corresponds to mammalian NEDL1, NEDL2. Present in molluscs; it has been lost in Platyhelminthes
HACE1		Not found	Not found	Only described in chordates so far.
HUWE1	***Smed-huwe1***	GAKN01012244.1	*Echinococcus* (1-2), *Taenia* (1), *Hymenolepis* (1), *Schistosoma* (1-2), *Procotyla* (1), *Dugesia* (1)	
KIAA0317		Not found	Not found	Present in molluscs; it has been lost in Platyhelminthes.
UBE3A/E6-AP		Not found	*Echinococcus* (0), *Taenia* (1), *Hymenolepis* (0), *Schistosoma* (1), *Procotyla* (1), *Dugesia* (0)	Either a recent loss in *Schmidtea* or still not sequenced
HECTX		Not found	Not found	Present in just a few animal species.
HECTD2		Not found	Not found	Present in molluscs, it has been lost in Platyhelminthes
SMALL HERCs	***Smed-sherc-1***	GAKN01018017.1	*Echinococcus* (2), *Taenia* (1), *Hymenolepis* (1), *Schistosoma* (1), *Procotyla* (2), *Dugesia* (0)	Corresponds to the orthologs of mammalian HERC3, HERC4, HERC5 and HERC6. The *Schmidtea* duplicates emerged very recently
	Smed-sherc-2	GAKN01009931.1		
UBE3B/3C	***Smed-ube3b***	GAKN01015216.1	*Echinococcus* (1), *Taenia* (1), *Hymenolepis* (1), *Schistosoma* (1), *Procotyla* (1), *Dugesia* (0)	
UBE3B/3C	***Smed-ube3c***	GAKN01016992.1	*Echinococcus* (1), *Taenia* (0), *Hymenolepis* (1), *Schistosoma* (1), *Procotyla* (1), *Dugesia* (0)	
TRIP12	***Smed-trip12***	GAKN01001286.1	*Echinococcus* (1), *Taenia* (1), *Hymenolepis* (0), *Schistosoma* (1), *Procotyla* (1), *Dugesia* (1)	
HECTD1	***Smed-hectd1-1***	GAKN01005514.1	*Echinococcus* (0), *Taenia* (2), *Hymenolepis* (0), *Schistosoma* (1), *Procotyla* (1), *Dugesia* (1)	
HECTD1	***Smed-hectd1-2***	GAKN01003620.1		Appears to be absent in all other species. *Taenia* also has two genes due to an independent duplication
EDD/UBR5	***Smed-ubr5***	GAKN01005557.1	*Echinococcus* (1), *Taenia* (0), *Hymenolepis* (1), *Schistosoma* (1), *Procotyla* (1), *Dugesia* (0)	
G2E3		Not found	Not found	Present only in chordates
KIAA0614		Not found	Not found	Present in molluscs; it has been lost in Platyhelminthes
HECTD3		Not found	Not found	Present in molluscs; it has been lost in Platyhelminthes
LARGE HERCs	***Smed-herc1***	GAKN01015423.1	*Echinococcus* (0), *Taenia* (0), *Hymenolepis* (0), *Schistosoma* (0), *Procotyla* (1), *Dugesia* (0)	
LARGE HERCs	***Smed-herc2***	GAKN01014599.1	*Echinococcus* (0), *Taenia* (0), *Hymenolepis* (0), *Schistosoma* (0), *Procotyla* (1), *Dugesia* (1)	
Not in any subfamily	***Smed-hect-like***	GAKN01017574.1	*Echinococcus* (0), *Taenia* (0), *Hymenolepis* (0), *Schistosoma* (0), *Procotyla* (1), *Dugesia* (0)	Divergent. Could not be assigned to any subfamily. Present only in *Procotyla* and *Schmidtea*

[a] Some of the reported absences may be due to lack of data. For example, *Procotyla* and *Schmidtea* have almost identical sets of HECT genes, while *Dugesia*, which is a closer relative of *Schmidtea*, lacks many.

sensitive population 2; X2), and the differentiated cell population (irradiation-insensitive; Xins) (Romero et al., 2012).

Microscopy and cell counting

Images of live animals and animals processed for *in situ* hybridization were captured with a Leica DFC290 camera mounted on a Leica M205 microscope. Fluorescent images were acquired using an Axiocam MRm camera mounted on a Zeiss Axio Observer. Z1 equipped with an ApoTome or a Zeiss SteREO Lumar V.12, or acquired using a Zeiss LSM 710 Confocal Microscope. Double fluorescent images are displayed as maximum image projections from ≤ 1 µm optical sections. For all experiments, we counted cells manually in ImageJ Software (Schneider et al., 2012), and biological replicates ($n \geq 2$) were averaged and reported as the mean $\pm$ s.d.

Reverse transcription quantitative PCR

Reverse transcription quantitative PCR (RT-pPCR) was performed on a Bio-Rad CFX Connect Real-Time System using SsoAdvanced SYBR Green Supermix (Bio-Rad) as described in (Cowles et al., 2014). The relative amount of each cDNA target was normalized to *Smed-GAPDH* (accession no. AY068133). The normalized relative changes in gene expression were calculated in Bio-Rad CFX Manager Software v3.0. Primers are listed in Table S1.

Results

Identification of HECT-domain E3 ubiquitin ligase genes in S. mediterranea

HECT-domain sequences have been used to classify genes of the HECT family in both animals and plants (Marín, 2010, 2013). To identify *S. mediterranea* genes predicted to encode HECT-containing ubiquitin ligases we used the HECT domains of multiple human genes as queries in database searches. The human sequences that were selected included members of the 16 HECT subfamilies in metazoans (Marín, 2010). In the *S. mediterranea* genome, we identified 17 HECT-domain containing genomic sequences predicted to encode for functional proteins. Of these 17 HECT sequences in *S. mediterranea*, 16 could be classified into established HECT subfamilies by phylogenetic comparison with 877 HECT domains from across the Animal Kingdom (see the section "Materials and methods"); one sequence (*Smed-hect-like*) was too divergent from known subfamilies to be classified into a HECT subfamily (Table 1). The HECTD1, small HERC, large HERC, and UBE3B/C subfamilies were represented by two sequences each in *S. mediterranea*. Five sequences appeared to be members of the NEDD4 HECTs (one from NEDD4a, three from NEDD4b, and one from NEDD4c subfamilies); HUWE1, TRIP12, and EDD/UBR5 subfamilies were each represented by one *S. mediterranea* gene. Nine HECT subfamilies (G2E3, HACE1, HECTD2, HECTD3, HECTX, KIAA0317, KIAA0614, NEDD4d, and UBE3A/E6-AP) were not found in the *S. mediterranea* genome. Planarian genes were named after the closest ortholog with two exceptions. The small HERC subfamily duplicates were renamed as "*small herc*" (*sherc-1* and *-2*) because the direct ortholog to human *herc3*, *herc4*, *herc5*, or *herc6* could not be resolved. The three NEDD4b subfamily members, all recent duplicates of each other, were named "*wwp1-like*". Suffixes -1, -2, or -3 were added for duplicated genes; "*Smed-*" prefixes were henceforth omitted for brevity.

Based on analyses using three different phylogenetic reconstruction methods (see the section "Materials and methods"), *S. mediterranea* lacks seven genes present before the protostome/deuterostome split; whereas, five new genes have appeared within Platyhelminthes (Fig. 1B). Thus, roles for a majority of planarian HECT genes may correspond to the more ancestral, basic functions of these same gene orthologs in higher organisms, including humans.

HECT genes are expressed in diverse planarian tissues

To analyze which tissues express planarian HECT genes, we performed WISH experiments. We found that all but two HECT genes were expressed throughout the parenchyma (mesenchyme) of the animal. The exceptions were *nedd4* and *hect-like*, which were only observed in the pharynx or in discrete peri-pharyngeal cells, respectively (Fig. S1). Of the 15 genes detected in the mesenchyme, *hectd1-1*, *sherc-1*, *sherc-2*, and *wwp1-like-1* were also expressed in the pharynx, discrete cells throughout the animal, peri-pharyngeal cells, and the intestinal branches, respectively (Fig. S1). Seven HECT-domain genes (*huwe1*, *trip12*, *ube3b*, *ube3c*, *ubr5*, *wwp1-like-2*, and *wwp1-like-3*) were detected in the cephalic ganglia and/or in the two ventral nerve cords comprising the central nervous system (CNS) (Fig. S1). These expression patterns suggest distinct roles for members of this gene family.

Previous transcriptome analysis of the planarian stem cell populations (Labbé et al., 2012; Önal et al., 2012) indicate that 15 HECT genes are expressed in the neoblasts (summarized in Fig. S2A). Thus, we performed WISH on planarians that had been γ-irradiated, a treatment that ablates the stem cell and progenitor cell populations (Eisenhoffer et al., 2008; Reddien and Sánchez Alvarado, 2004). These experiments showed that expression of 11 of the 17 HECT domain genes could be readily detected in irradiation-sensitive cell populations (Fig. S1). Six genes, *hectd1-2*, *huwe1*, *sherc1*, *smurf*, *trip12*, *ube3c*, displayed decreased expression 3 days after γ-irradiation treatment and 5 additional genes, *herc1*, *herc2*, *sherc2*, *ubr5*, *wwp1-l1*, showed a decrease in signal intensity 5 days after irradiation, suggesting the first group of genes was expressed in neoblasts and/or their early progeny whereas the second group was likely expressed in late progeny. Combined, these studies suggest HECT E3s might have roles in stem cell regulation. We next asked if any of these genes function in stem cell maintenance or differentiation.

sherc-1 is expressed in early neoblast progeny

The expression pattern of *sherc-1* was similar to the irradiation-sensitive pattern observed for the stem cell progeny markers *prog-1*, *prog-2*, *and agat-1* (*NB.21.11e*, *NB.32.1g*, and *NB.8.8b*, respectively) (Eisenhoffer et al., 2008) (Fig. 2A), which were recently assigned to epidermal-lineage cell types (van Wolfswinkel et al., 2014). Therefore, we asked if *sherc-1* was also expressed in these cell populations using double fluorescent *in situ* hybridization (dFISH) to *sherc-1* and epidermal cell lineage-specific genes. Co-expression of *sherc-1* with the neoblast marker *smedwi-1* was observed at a low frequency (6.7 $\pm$ 3.3%, Fig. 2B). By contrast, *sherc-1* was highly expressed in a population of early progeny cells, seen with co-labeling by *prog-2* (70.4 $\pm$ 8.6%, Fig. 2C). We rarely detected *sherc-1*$^+$ cells labeled with the late progeny marker *agat-1* (3.0 $\pm$ 0.2%, Fig. 2D). Thus, our data clearly indicate *sherc-1* expression is primarily restricted to a large fraction of early progeny cells also marked by *prog-2*. Additional experiments will be required to determine if *sherc-1* is dynamically expressed during early neoblast progeny specification, as neoblasts transition to late progeny, or if this gene defines a specialized subset of *prog-2*$^+$ cells. van Wolfswinkel et al. (2014) identified two broad neoblast classes they termed σ- and ζ-neoblasts. The ζ-neoblasts give rise to post-mitotic lineages, including epidermal cells. It will be interesting to determine if *sherc-1*$^+$/*smedwi-1*$^+$ cells are also

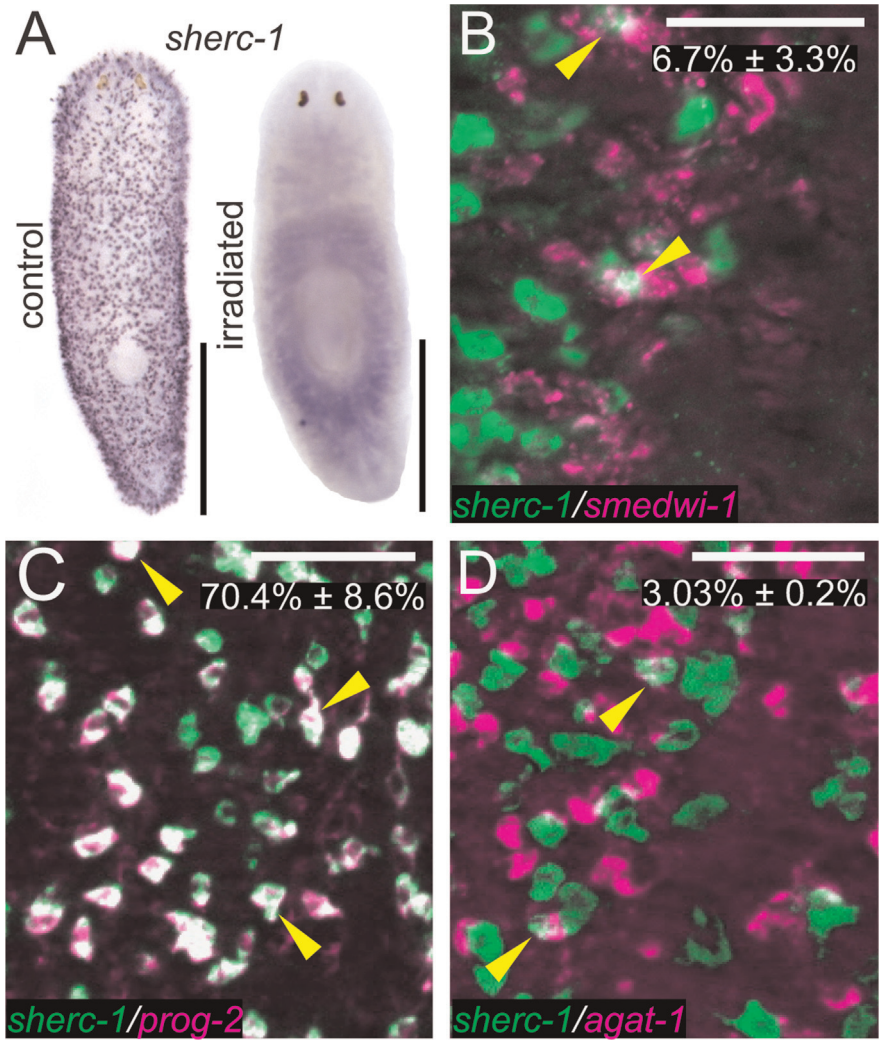

Fig. 2. *sherc-1* is expressed in neoblast progeny. (A) Expression pattern of *sherc-1* in representative control and γ-irradiated animals ($n=14$). (B) Co-expression of *sherc-1* and *smedwi-1* analyzed by double fluorescent *in situ* hybridization (dFISH) ($n=348$ cells, 3 animals). Yellow arrowheads indicate cells expressing both genes (white). (C) Representative dFISH analysis of *sherc-1* and *prog-2* expression ($n=634$ cells, 3 animals). Yellow arrowheads point to *sherc-1*$^+$/*prog-2*$^+$ cells. (D) Representative dFISH image demonstrating expression of *sherc-1* and *agat-1* ($n=351$ cells, 3 animals). Scale bars: (A) 500 μm; (B–D) 100 μm.

positive for the ζ-neoblast marker *zfp-1* and whether *sherc-1* plays a role in ζ-neoblast regulation.

Functional analysis of planarian HECT E3 ligases

In order to investigate if HECT E3s play roles in adult stem cells or regeneration, we inhibited their expression using RNAi. Planarians were fed either bacterially-expressed dsRNA targeting *green fluorescent protein* as a control (referred to as *control(RNAi)*), or a single HECT gene, twice a week for 4–8 weeks. We also performed double knockdown against predicted paralogs: *hectd1-1,-2 (RNAi), sherc-1,-2(RNAi)*, and *wwp1-like-2,-3(RNAi)*. First, we tested each experimental group for the ability to regenerate all tissues by amputating the head or the tail; regeneration of these structures takes 1–2 weeks and depends on the proliferation and differentiation of the neoblasts to form a regeneration blastema and replace missing tissues (Agata and Watanabe, 1999; Newmark and Sánchez Alvarado, 2002; Sánchez Alvarado, 2007). We then inspected the animals for any effects on stem cell and progeny populations, using cell-type specific markers in uninjured animals (described below). This initial screen revealed three distinct phenotypes as the result of single RNAi knockdown experiments against *trip12*, *huwe1*, or *wwp1-like-1* (hereon referred to as *wwp1*), which are described below.

trip12 functions in posterior regeneration

WISH showed *trip12* was broadly expressed throughout the mesenchyme of the animal, CNS, and irradiation-sensitive cells (Fig. 3A). When we knocked down *trip12* and amputated the animals, we observed that *trip12(RNAi)* planarians were capable of regenerating new heads (Fig. 3B). Surprisingly, 25% of RNAi knockdown animals healed the wounds and formed blastemas, but failed to restore a tail (Fig. 3C). Consistent with this inability to regenerate tails, we also noted that 39% of intact *trip12(RNAi)* planarians lost their tails over the course of 8 weeks (Fig. 3D). These results suggested that *trip12* plays a role in establishing and maintaining posterior/tail identity. In addition to the loss-of-tail phenotype, we noticed some abnormal behaviors such as abnormal phototaxis and inching movements in *trip12(RNAi)* animals (not shown). Combined, our data suggest that inhibition of *trip12* results in pleiotropic effects, which is consistent with the broad expression pattern of *trip12* and that it likely has multiple targets involved in different cellular processes.

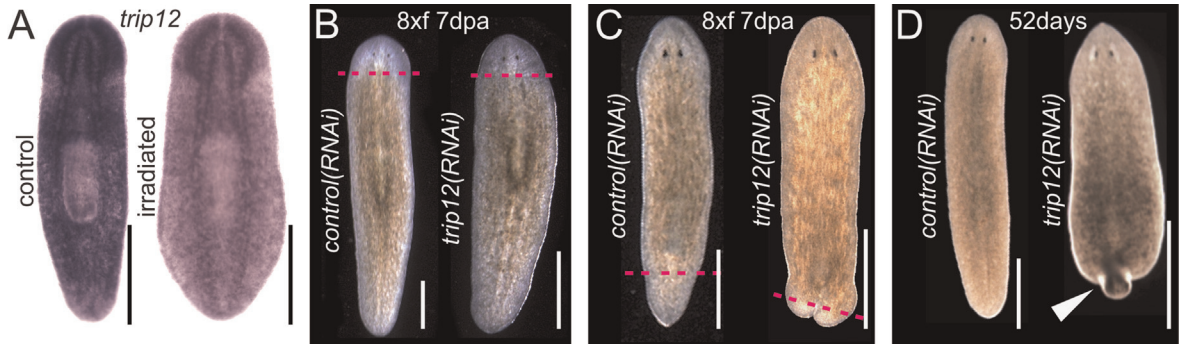

Fig. 3. RNAi knockdown of *trip12* inhibits tail regeneration and maintenance. (A) Expression of *trip12* in control and irradiated animals ($n=14$ and 9, respectively). (B–C) Representative image of animals fed control or *trip12* dsRNA eight times (8xf) seven days post-amputation (7 dpa). Similar to the controls, *trip12(RNAi)* animals regenerated heads. The inability to regenerate tails was observed in 36 of 147 *trip12(RNAi)* animals at 7 days post amputation (7 dpa). Magenta dashed line indicates amputation site. (D) Image of intact planarians treated with control or *trip12* dsRNA. *trip12(RNAi)* planarians failed to maintain posterior tissues (phenotype observed in 62 of 158 animals after 52 days of RNAi). White arrowhead indicates regression of tail tissue. Scale bars: (A) 500 μm; (B–D) 1 mm.

huwe1 plays a crucial role in neoblast proliferation control

huwe1 mRNA was detected throughout the animal in both irradiation-sensitive and insensitive cells (including the cephalic ganglia and ventral nerve cords) (Fig. 4A), suggesting potential roles in stem cell and CNS function. To confirm *huwe1* is a neoblast-expressed gene, we examined if *huwe1* RNA could be detected in *smedwi-1*$^+$ neoblasts by dFISH and observed cells that expressed both of these transcripts (Fig. 4B). In addition, we verified expression of *huwe1* in stem cells by RT-qPCR (Fig. S2B). Combined with previous reports (Fig. S2A), our data suggests that *huwe1* is expressed in neoblasts or early progeny.

Because HUWE1 (also known as ARF-BP1, Mule, or HectH9) is known to target several cell cycle regulators (Bernassola et al., 2008; Inoue et al., 2013), we hypothesized that *huwe1* is required for neoblast regulation in planarians and that knockdown of *huwe1* would impair their ability to regenerate. Indeed, we found that amputated *huwe1(RNAi)* animals were able to heal the wound but failed to grow blastemas or regenerate missing tissues (Fig. 4C). In addition, we noted both regenerate and uninjured *huwe1(RNAi)* planarians displayed a bloated phenotype (Fig. 4C) and did not display normal negative phototaxis (data not shown). We also observed a marked decrease in the length of uninjured animals compared to the controls (Fig. 4D); both intact and regenerating *huwe1(RNAi)* animals died by 18 days after the final RNAi feeding (Fig. 4E).

Based on the lethal phenotype and expression pattern, we reasoned that knockdown of *huwe1* caused a profound defect in stem cell regulation and further analyzed the neoblast population in uninjured *huwe1(RNAi)* planarians. Compared to the controls, we observed a dramatic increase in the expression of *smedwi-1* mRNA and number of anti-phosphohistone-H3$^+$ (PH3$^+$) cells in *huwe1* RNAi planarians 1 week after 8 RNAi feedings (Fig. 5A and B). These results suggested inhibition of *huwe1* led to neoblast hyperproliferation; therefore, we tested for incorporation of the thymidine analog bromodeoxyuridine (BrdU) to analyze the population of cells entering S-phase. Animals that were fed *huwe1* dsRNA 6 times, which was the earliest time point to show a phenotype in our experiments, and then soaked for 1 h in BrdU showed a dramatic increase in anti-BrdU staining after a 2 h chase, indicating that a higher proportion of the neoblasts were in S-phase (Fig. 5C and C′). However, an increase in BrdU staining could also indicate that cell cycle dynamics are altered in *huwe1*-deficient planarians. Thus, we next analyzed cell populations by flow cytometry on dissociated animals. In contrast to the controls, flow cytometry showed a striking increase in the total number of cells within the γ-irradiation sensitive (X1) compartment in *huwe1(RNAi)* animals (Fig. 5D). Finally, because *huwe1* knockdown eventually caused death, we also asked what effect *huwe1* RNAi had on apoptosis. Using TUNEL to assay for apoptotic cell death we observed a global increase in TUNEL$^+$ cells in *huwe1(RNAi)* animals (Fig. 5E and E′). We do not know what cell types were TUNEL$^+$, but we hypothesize they may be differentiating or differentiated cells.

In summary, inhibition of *huwe1* expression resulted in an increased neoblast population, bloating, shrinking, and blocked regeneration following amputation. Our data indicate that *huwe1* functions in the neoblasts to regulate the decision to proliferate and cell cycle progression. In the absence of *huwe1*, uncontrolled proliferation led to increased apoptosis and death. We conclude *huwe1* is indispensable for homeostatic control and regeneration in planarians.

wwp1 is required for regeneration, stem cell maintenance, and intestinal regulation

Our analysis showed *wwp1* was prominently expressed in the intestine and throughout cells in the mesenchyme (Fig. 6A). Consistent with the strong expression in the intestine, RNA-seq data indicate that *wwp1* is enriched in differentiated tissues (Labbé et al., 2012; Önal et al., 2012); however, these studies also reported *wwp1* expression in both the neoblast and progeny populations, albeit at lower levels (Fig. S2A). We performed dFISH to *wwp1* and *smedwi-1* but were unable to reliably detect *wwp-1* with our current technique (data not shown). However, we were able to detect *wwp1* expression in the neoblasts by RT-qPCR, consistent with previous reports (Fig. S2B). Our data suggest that *wwp1* could have roles in both the neoblasts and intestine of planarians. Therefore, we proceeded to examine the effect of *wwp1* knockdown on both cell types.

Animals fed dsRNA targeting *wwp1* exhibited incomplete regeneration, formed dorsal tissue lesions (Fig. 6B), and were less responsive to stimuli such as light or gentle agitation that normally induce movement (data not shown). Analysis of the stem cell population revealed an increase in the number of PH3$^+$ cells in *wwp1(RNAi)* animals compared to controls (Fig. 6C). It has been previously reported that WWP1 promotes proliferation and loss of WWP1 leads to a decrease in DNA synthesis and cell growth in cancer cell lines (Chen et al., 2007). We reasoned the increase in PH3 staining in planarians could also be due to defects in cell cycle progression. To test this possibility, we incubated animals with BrdU to determine if the increase in mitosis was a consequence of more stem cells entering S-phase, however, we observed a reduction in the number of BrdU$^+$ cells in *wwp1(RNAi)* animals (Fig. 6D). We next reasoned that delays in cell cycle progression

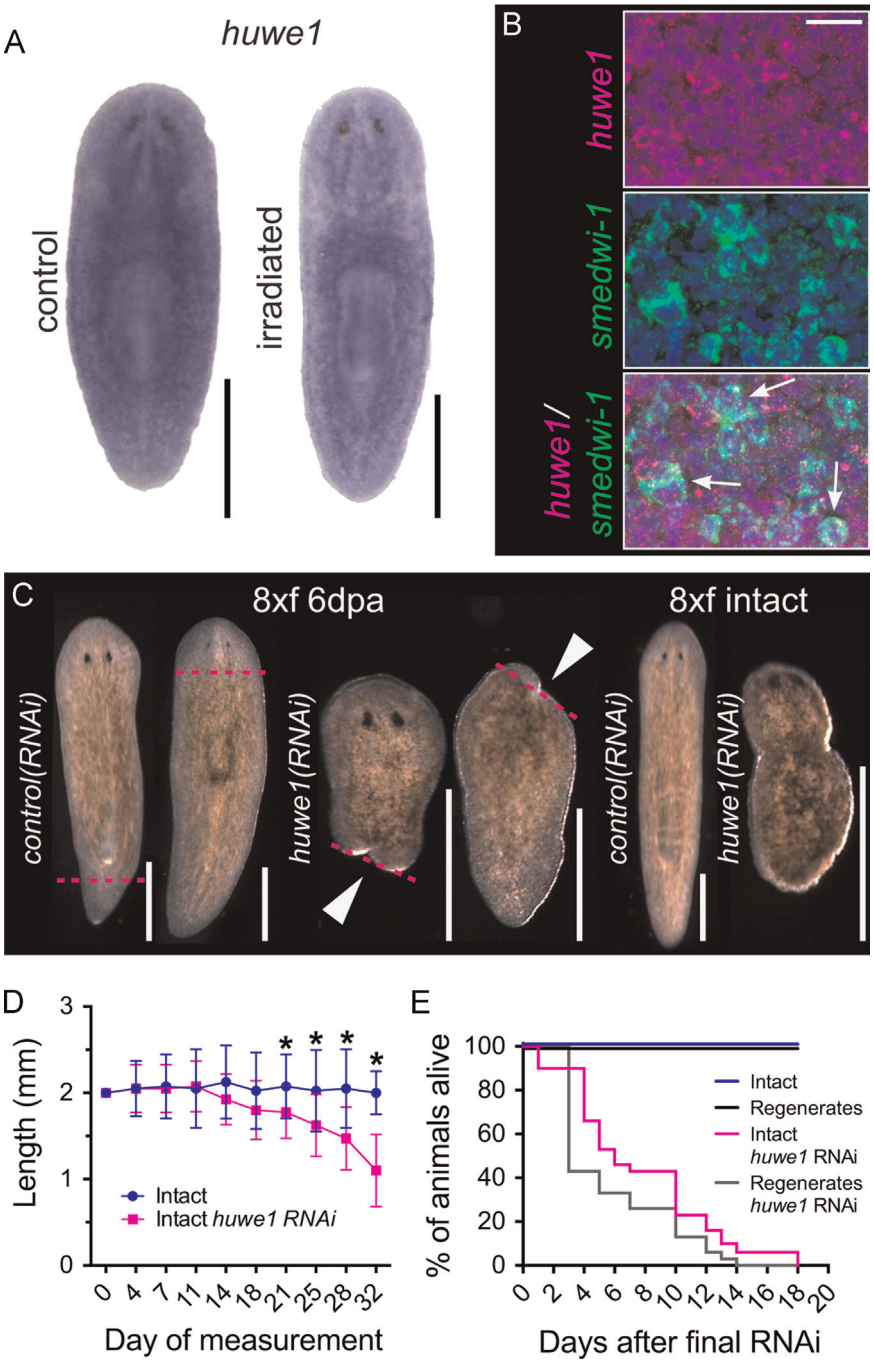

Fig. 4. The function of *huwe1* is essential for regeneration. (A) *In situ* hybridization to *huwe1* in control and γ-irradiated planarians ($n=13$ and 8, respectively). (B) Analysis of co-expression of *huwe1* and *smedwi-1*. White arrows indicate cells expressing both genes. (C) Representative image of *huwe1(RNAi)* animal that was fed dsRNA 8 times at 6 days post-amputation (8xf 6 dpa; phenotype observed in 10 of 12 animals) or uninjured animal showing bloating phenotype (8xf intact; phenotype observed in 12 of 12 animals). White arrowheads indicate lack of blastemas; magenta dashed line indicates amputation site. (D) Graph of animal length measured over course of an RNAi timecourse. Planarians were measured a day prior to the first RNAi feeding (day 0) and subsequent RNAi treatments (9 feedings in total). There were 20 animals measured per treatment except days 28 ($n=17$ in *huwe* RNAi) and 32 ($n=9$ in the intact controls and 5 in *huwe* RNAi). Graph shows the mean ± s.d. $^{*}P<0.05$, Student's *t*-test. (E) Survival curve of intact or regenerating planarians treated with control or *huwe1* dsRNA. Day "0" marks the first day of survival analysis following completion of the ninth RNAi feeding ($n=20$ animals per group). Scale bars: (A) 500 μm; (B) 20 μm; (C) 500 μm.

could trigger cell death. TUNEL staining revealed an increase in the number of TUNEL^{+} nuclei in *wwp1(RNAi)* planarians (Fig. 6E). Together our data suggest that loss of *wwp1* causes neoblasts to be stalled in M-phase and unable to complete the cell cycle, leading to an overall decrease in the neoblast population. Next, we estimated stem cell numbers by dissociating whole animals and quantifying neoblast, progeny, and differentiated cell populations using flow cytometry; our analysis revealed that *wwp1(RNAi)* animals had lost most of the cycling neoblast population (X1) compared to the controls (4.65% vs. 15.25%, Fig. 6F). We conclude that loss of *wwp1* leads to a decrease in the neoblast population.

To investigate the function of *wwp1* in the intestine we examined the expression of intestinal-specific genes in *wwp1 (RNAi)* animals. We found detection levels of mRNA for the transcription factor *nkx2.2* (Forsthoefel et al., 2012) and the gap junction gene *inx9* (Oviedo and Levin, 2007) were decreased in *wwp1(RNAi)* planarians after 12 and 20 RNAi feedings, respectively (Fig. 7A, B). To visualize intestinal morphology, we labeled

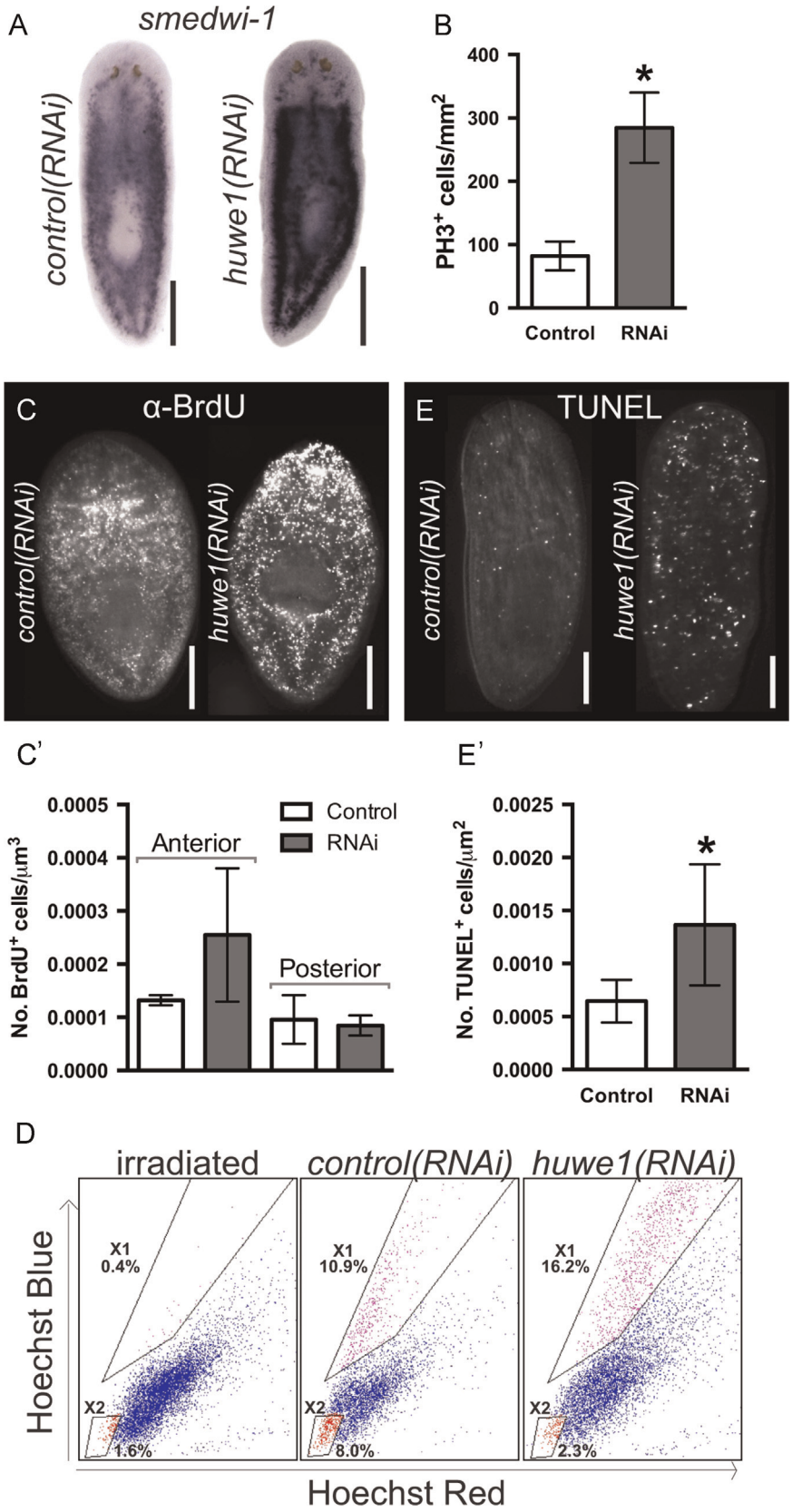

Fig. 5. *huwe1* regulates neoblast proliferation. (A) Representative images of planarians that were fed control or *huwe1* bacterially expressed dsRNA 8 times over 4 weeks, fixed 1 week after the final feeding, and processed for *in situ* hybridization to *smedwi-1* side-by-side and developed for the same length of time. Differential expression observed in 4 of 4 animals at 8xf and 4 of 4 animals at 7xf. (B) Quantification of $PH3^+$ cells per mm^2 ($p=0.0001$, $n=5$). Animals were fixed 1 week after 8 dsRNA feedings. (C) Image of control and *huwe1* knockdown animals RNAi-treated 6 times, starved 1 week, soaked in BrdU for 1 h and fixed 2 h later and processed for BrdU staining (αBrdU) ($n=3$). (C′) Quantification of $BrdU^+$ cells in $212 \times 212\ \mu m^2$ regions immediately anterior and posterior to the pharynx and normalized by the volume. (D) Representative graphs of flow cytometry analysis performed on animals 1 week after 6, 7, or 8 *huwe1* dsRNA feedings. X1 represents a population of cells highly sensitive to γ-irradiation (neoblasts and progeny, purple dots); X2 represents a population of cells less sensitive to γ-irradiation (progeny, red dots). Blue dots represent the irradiation-insensitive cell population (differentiated cells). *huwe1(RNAi)* sample after 8 dsRNA feedings shows a ~6% increase in the X1 population compared to controls. Irradiated sample was used to set gates. Values represent the means calculated from two independent experiments. (E) Representative image of animals fed dsRNA 6–7 times, starved 1 week and processed for TUNEL staining ($n=5$). (E′) Quantification of $TUNEL^+$ cells in whole animals normalized by the area of the worm. Graphs show the mean ± s.d. $^*P<0.05$, Student's *t*-test. Scale bars: (A) 200 μm; (E) 100 μm.

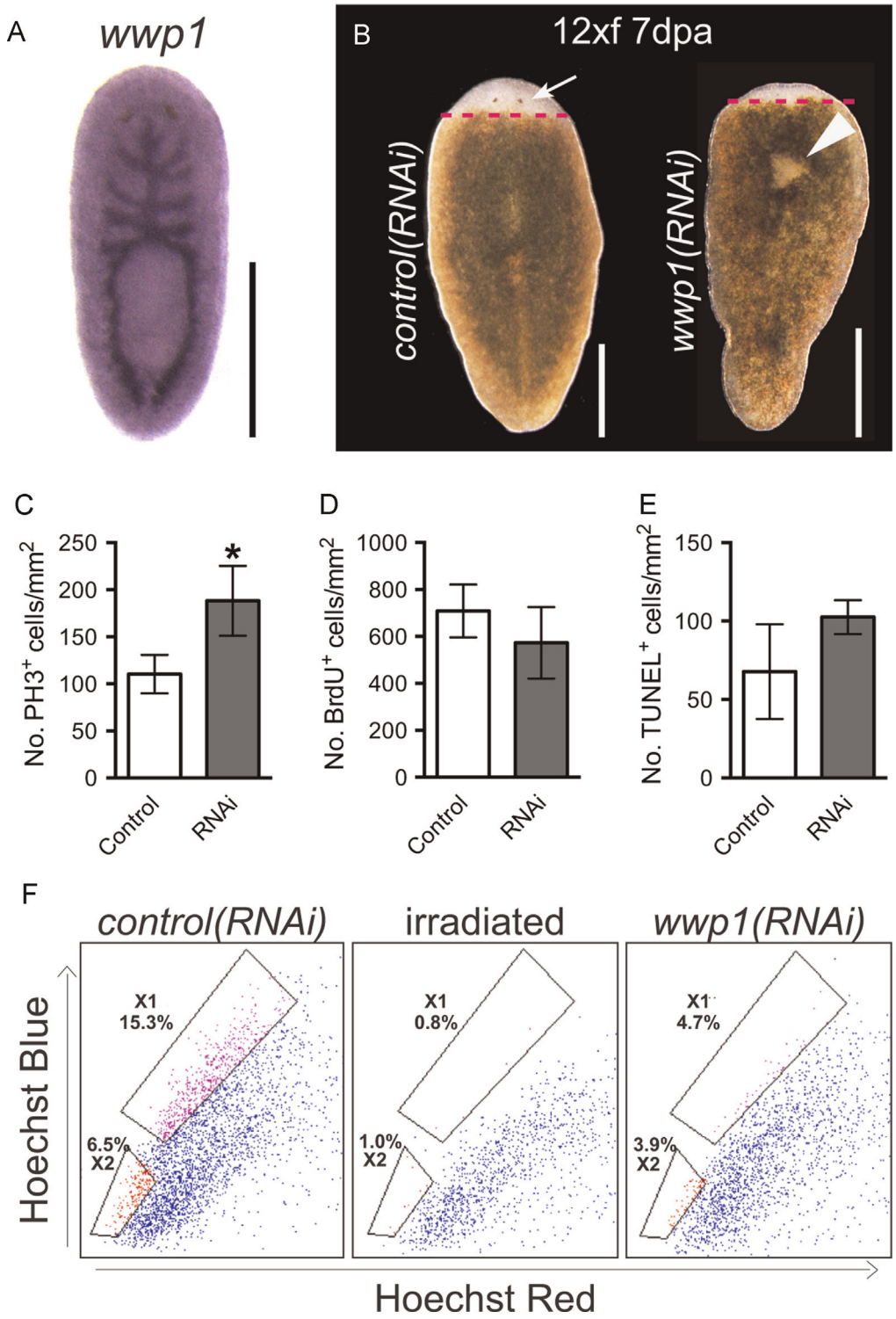

Fig. 6. Expression of *wwp1* is required for neoblast maintenance and tissue regeneration. (A) *In situ* hybridization to *wwp1* in intact planarians ($n=18$). (B) Representative image of *wwp1(RNAi)* animal at 7 days post-amputation (7 dpa). Animals were fed *wwp1* dsRNA 12 times (12xf) over 6 weeks and amputated the day after 12th feeding. Magenta dashed line indicates amputation site. White arrow indicates normal blastemas and photoreceptor regeneration in control compared to *wwp1(RNAi)* animals (phenotype observed in 17/20 animals). White arrowhead indicates tissue lesions in *wwp1(RNAi)* animals (observed in 14/20 animals). (C) Quantification of PH3$^+$ cells per mm^2 in control and *wwp1(RNAi)* animals ($p=0.0001$, $n=10$). (D) Quantification of BrdU$^+$ cells in *wwp1(RNAi)* and *control(RNAi)* animals ($n=5$). (E) Quantification of TUNEL$^+$ cells in *wwp1(RNAi)* and *control(RNAi)* animals ($n=4$). (F) Representative graphs of flow cytometry data. X1 represents neoblast and progeny populations highly sensitive to γ-irradiation (purple). X2 represents progeny populations less sensitive to γ-irradiation (red). Differentiated cells are represented in blue. Values represent the mean values calculated from two independent experiments. (C–E) Analyses were performed on 1 week starved intact animals fed dsRNA 12 times over 6 weeks. Graphs shows the mean ± s.d. $^*P<0.05$, Student's *t*-test. Scale bars: (A–B) 500 μm.

planarians with anti-3G9 (Forsthoefel et al., 2012), a monoclonal antibody specific to phagocytes (Fig. 7C), which revealed cells within the intestinal branches were noticeably disorganized following *wwp1* knockdown. Staining *wwp1(RNAi)* animals with markers for other tissues including the CNS (*chat*), protonephridia (*inx10*), or the pharynx (*laminin*), did not reveal obvious defects in

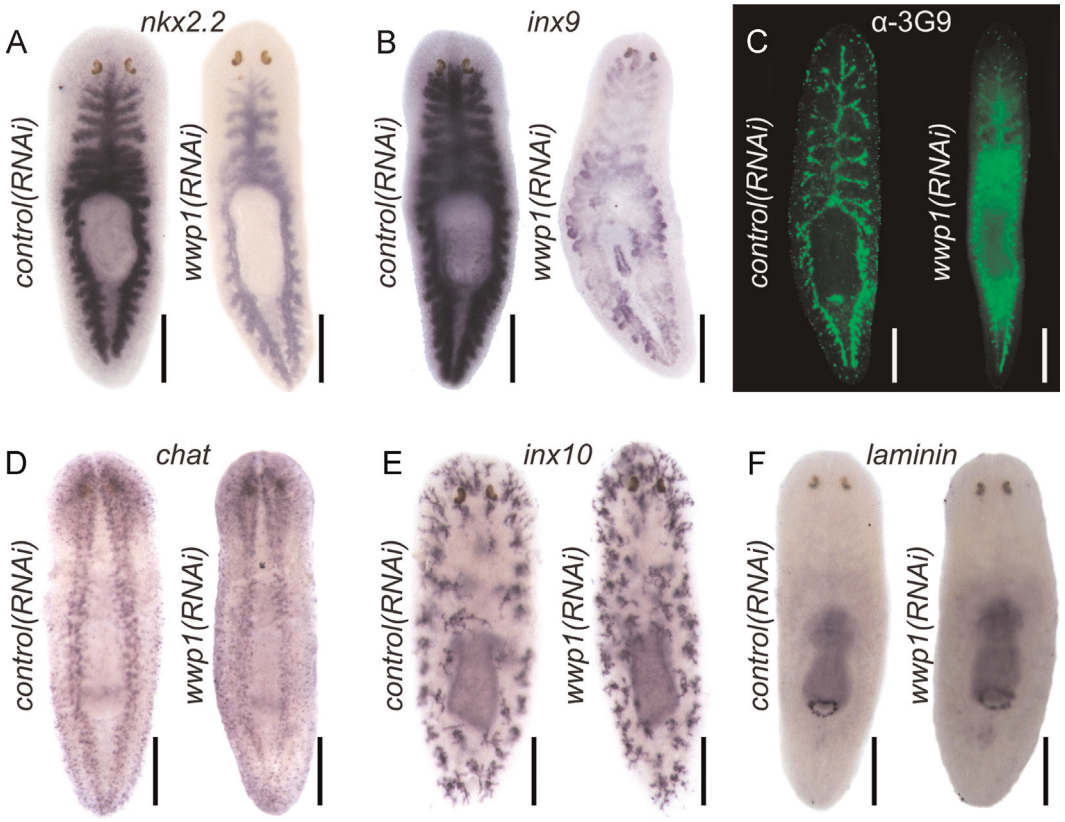

Fig. 7. Inhibition of *wwp1* leads to defects in intestinal integrity. (A–B) *In situ* hybridization on *wwp1(RNAi)* and *control(RNAi)* animals to detect *nkx2.2* (A; $n=4$, 12xf) or *inx9* (B; $n=4$, 20xf). (C) Staining of intestinal phagocytes with the monoclonal antibody 3G9 in *control* and *wwp1* RNAi planarians ($n=5$, 12xf). (D–F) *In situ* hybridization to *chat*, *inx10*, or *laminin* to label the CNS, protonephridia, and pharynx, respectively, in RNAi animals ($n=6$). All analyses were performed on 1 week starved intact animals (2–3 mm in length) that were fed dsRNA 12 or 20 times over 6 or 10 weeks, respectively. Samples were processed side-by-side and developed for the same amount of time for comparison purposes. Scale bars=200 μm.

these tissues (Fig. 7D–F). We conclude *wwp1* is also required to maintain proper intestinal morphology.

Discussion

In this study, we identified 17 HECT-domain genes in the planarian *S. mediterranea*. Our data suggest that the HECT family in Platyhelminthes has become simplified with only 10 of the 16 established subfamilies represented (Table 1); a similar pattern is seen in insect and urochordate lineages (Marín, 2010). Some genes appeared to be recent duplications, such as *sherc-1* and *-2*. A single highly divergent gene detected by our analysis, *hect-like*, appears to be planarian specific (found in *S. mediterranea* and *Procotyla fluviatilis*). With the exception of *hect-like*, all HECT-domain genes found in *S. mediterranea* are similar to HECT genes present in other animals. Known HECT E3 targets include key developmental proteins such as TGF-β, EGF, JNK, and Notch signaling components; KLF and Smad transcription factors; and PTEN and p53 family member tumor suppressors (Rotin and Kumar, 2009; Scheffner and Staub, 2007). Understanding the roles of *S. mediterranea* HECT E3 ligases may give clues to additional functions of their homologs in other organisms. We examined gene function using RNAi to screen the roles of these genes *in vivo*. We uncovered that three HECT genes, *trip12, huwe1*, and *wwp1*, had roles in regeneration and two, *huwe1* and *wwp1*, function in neoblast regulation.

trip12 is necessary for regeneration of posterior tissues

The role of *trip12* in planarians is intriguing. Although *trip12* expression was observed throughout the body of the animal, inhibition of *trip12* affected only regeneration of posterior tissues. A potential explanation for the loss-of-tail phenotype could be misregulation of genes implicated in axial polarity. Proteomic studies would be necessary to truly test if TRIP12 targets polarity genes such as WNT or β-Catenin. In planarians, *wnt1* is expressed in discrete cells located at the dorsoposterior midline in *S. mediterranea* (Petersen and Reddien, 2009; Reddien, 2011) and *Dugesia japonica* (Yazawa et al., 2009). In preliminary experiments, we did not detect changes in *wnt1* expression in *trip12*(*RNAi*) animals using WISH (data not shown), suggesting that *trip12* inhibition might not have an impact on the transcription of polarity genes; this intriguing possibility will need to be investigated further by performing RNAi timecourse experiments and assaying the expression of several posterior markers with quantitative methods such as RT-qPCR. Few TRIP12 targets have been identified to date and no proteins involved in tissue patterning have been hitherto identified. For example, human TRIP12, in conjunction with UBR5, plays a crucial role in the suppression of a histone ubiquitylating RING E3, RNF168, effectively controlling the spread of chromatin silencing (Gudjonsson et al., 2012). In addition, the transcription factor SOX6 was recently identified as a target of TRIP12 in mammals (An et al., 2013). SOX6 is responsible for the transcriptional repression of slow twitch muscle fiber genes. Whereas SOX6 may have adapted to this specific role in muscle cells in mammalian lineages, the family of SOX transcription factors have roles in differentiation of various cell types (Sarkar and Hochedlinger, 2013). It will be critical to identify TRIP12 targets in planarians to elucidate the role of this enzyme in posterior tissue maintenance and regeneration.

Additionally, mammalian TRIP12 plays a critical role in the regulation of *p53* expression *via* ubiquitin-mediated degradation of ARF (Chen et al., 2010). It remains to be investigated if ARF or other proteins that regulate p53 in planarians contribute to mitotic activity following *trip12* knockdown. Here, we did not investigate the function of *trip12* in the stem cell population but given this gene is also detected in neoblasts (Fig. S2), it will be interesting to examine which neoblast categories (van Wolfswinkel et al., 2014) express *trip12* and whether RNAi knockdown has a direct effect on stem cell function.

The function of HUWE1 in cell cycle regulation is conserved in planarians

Upon knockdown of *huwe1*, we observed hallmarks of hyperproliferation including increased mitosis, increased expression of the neoblast marker *smedwi-1*, increased BrdU$^+$ cells, and expanded neoblast population, strongly suggesting that this gene controls the cell cycle. HUWE1 has been implicated in regulating several protein targets required for cell cycle control. For example, HUWE1 targets P53 (Chen et al., 2005), p19Arf (Qi et al., 2012), BRCA1 (Wang et al., 2014), and N-Myc (D'Arca et al., 2010) for degradation in various cell lines and mouse models. Additionally, HUWE1 functions as a tumor suppressor *in vivo* based on experiments in mice (Inoue et al., 2013). Planarian tissues undergo constant homeostatic cell turnover and increased proliferation during regeneration of missing tissues, processes that require tight regulation of the cell cycle. Thus, these organisms provide an excellent model to investigate how HUWE1 regulates the cell cycle during stem cell self-renewal and differentiation. Tumor suppressors may have evolved in order to control proliferation during development (Pearson and Sánchez Alvarado, 2008) as well as to promote tissue regeneration (Pomerantz and Blau, 2013). RNAi experiments showed that *huwe1* was required for planarian regeneration (Fig. 4C), similar to the phenotypes observed after loss of p53 and PTEN in *S. mediterranea* (Oviedo et al., 2008; Pearson and Sánchez Alvarado, 2010). The *huwe1* RNAi phenotype was underscored by a dramatic increase in neoblasts (Fig. 5A–D). Thus, if we define tumor suppressors as factors that both suppress proliferation and enhance regeneration, our data demonstrate that *huwe1* acts as a tumor suppressor equivalent in planarians. Because *huwe1* is one of the more ancestral HECT-domain genes (Fig. 1B) and planarians may not possess all known HUWE1 targets, future studies should help to reveal proteins regulated by *huwe1* in planarians that are required for neoblast regulation. *huwe1* was also expressed in differentiated cells and might be required for normal differentiation. Future experiments will aim to decipher how HUWE1 functions in the neoblasts and what role it plays in differentiation.

wwp1-like-1 has roles in intestinal integrity and neoblast maintenance

We identified three genes that shared similarity with WWP1 in *S. mediterranea*. RNAi knockdown of *wwp1-like-2* and *-3* did not result in overt regeneration phenotypes. We also performed *wwp1-like-2,-3(RNAi)* double knockdown experiments because these two genes had similar expression patterns (Fig. S1); however, we did not observe any effects compared to single knockdowns. By contrast, *wwp1-like-1* (*wwp1*) RNAi planarians were unresponsive to external stimuli, exhibited delayed regeneration, formed lesions, and lysed following amputation. Interestingly, wound healing and blastema formation were normal in these animals; however, regeneration was inhibited by 5 days post-amputation. Our results suggest that *wwp1* is not required for wound healing but functions in the later stages of regeneration, including proliferation, cell migration, and differentiation (Reddien and Sánchez Alvarado, 2004). Current evidence links WWP1 to differentiation of human osteoblasts (Zhi and Chen, 2012), thus, *wwp1* could have a conserved function in differentiation of other cell types in planarians.

We observed strong expression of *wwp1* in the planarian intestine and found that inhibition of *wwp1* led to death in an otherwise "immortal" animal (Sánchez Alvarado, 2004). Expression of *wwp1* in intestinal cells was also reported in *Caenorhabditis elegans* and overexpression of *wwp1* was shown to regulate diet-restricted longevity leading to increased lifespan (Carrano et al., 2009). Human WWP1 is overexpressed in certain carcinomas (Subik et al., 2012), supporting the idea that it promotes longevity or cell proliferation. Recently, it was demonstrated that the function of WWP1 in *C. elegans* is mediated by ubiquitylation of KLF-1 (Carrano et al., 2014). Future experiments should determine if *wwp1* also functions together with a *Krüppel-like factor* to regulate longevity in *S. mediterranea* or if a novel mechanism exists in planarians. In addition, *wwp1*(*RNAi*) animals showed a decrease in the neoblast population. Recent evidence suggests that the intestine might serve as a neoblast niche (Forsthoefel et al., 2012); thus, inhibition of *wwp1* function in the intestine might also underlie neoblast regulation defects.

In human fibroblasts, WWP1 targets p27^{kip1} for degradation (Cao et al., 2011), potentially causing a halt in the cell cycle. However, a planarian homolog of p27^{kip1} has not been identified. It is possible the loss of neoblasts was underscored by defective cell cycle progression or cell growth, but we do not yet know the exact mechanism leading to increased PH3$^+$ and TUNEL$^+$ cells. Inhibition of *wwp1* expression had pleiotropic effects, suggesting that different targets may be responsible for the different effects seen on the neoblasts and intestine. Identification of the targets of WWP1 may reveal a cell cycle regulator with roles similar to p27^{kip1} or alternative substrates regulating the cell cycle in *S. mediterranea*.

Conclusions

Our work on the family of HECT E3 ligases in *S. mediterranea* has revealed roles for a subset of HECT-domain encoding genes in tissue regeneration and stem cell regulation. The pleiotropic yet distinct phenotypes observed by our gene knockdown experiments highlights the broad range of specific targets each HECT E3 affects. The phenotypes that followed inhibition of *trip12*, *huwe1*, and *wwp1* could serve as readout for downstream analysis and identification of target E3 ubiquitin ligase substrates in specific biological contexts. Therefore, future experiments will test the effect of RNAi knockdown on global ubiquitylated protein levels to determine if planarians may be used as a tool for future proteomic studies aimed at screening for candidate protein targets of E3 ubiquitin ligases implicated in regenerative processes.

Acknowledgments

We thank Ionit Iberkleid and Kelly Ross for helpful comments on the manuscript; Martis Cowles for technical advice, sharing reagents, and providing RNA from FACS isolated planarian cells for RT-qPCR experiments; and Bret Pearson for providing the planarian Instant Ocean Sea Salts protocol. The authors acknowledge the San Diego State University Flow Cytometry Core Facility for assistance with sample analysis. This work was funded by a California Institute for Regenerative Medicine Grant RN2-00940-1 and NSF IOS-1350302.

Appendix A. Supplementary material

Supplementary data associated with this article can be found in the online version at http://dx.doi.org/10.1016/j.ydbio.2015.04.021.

References

Adell, T., Cebrià, F., Saló, E., 2010. Gradients in planarian regeneration and homeostasis. Cold Spring Harb. Perspect. Biol. 2, a000505.

Agata, K., Watanabe, K., 1999. Molecular and cellular aspects of planarian regeneration. Semin. Cell Dev. Biol. 10, 377–383.

An, C.I., Ganio, E., Hagiwara, N., 2013. Trip12, a HECT domain E3 ubiquitin ligase, targets Sox6 for proteasomal degradation and affects fiber type-specific gene expression in muscle cells. Skelet. Muscle 3, 11.

Ardley, H.C., Robinson, P.A., 2005. E3 ubiquitin ligases. Essays Biochem. 41, 15–30.

Bernassola, F., Karin, M., Ciechanover, A., Melino, G., 2008. The HECT family of E3 ubiquitin ligases: multiple players in cancer development. Cancer Cell 14, 10–21.

Boser, A., Drexler, H.C.A., Reuter, H., Schmitz, H., Wu, G.M., Scholer, H.R., Gentile, L., Bartscherer, K., 2013. SILAC proteomics of planarians identifies Ncoa5 as a conserved component of pluripotent stem cells. Cell Rep. 5, 1142–1155.

Cao, X., Xue, L., Han, L., Ma, L., Chen, T., Tong, T., 2011. WW domain-containing E3 ubiquitin protein ligase 1 (WWP1) delays cellular senescence by promoting p27 (Kip1) degradation in human diploid fibroblasts. J. Biol. Chem. 286, 33447–33456.

Carrano, A.C., Dillin, A., Hunter, T., 2014. A kruppel-like factor downstream of the E3 ligase WWP-1 mediates dietary-restriction-induced longevity in *Caenorhabditis elegans*. Nat. Commun. 5, 3772.

Carrano, A.C., Liu, Z., Dillin, A., Hunter, T., 2009. A conserved ubiquitination pathway determines longevity in response to diet restriction. Nature 460, 396–399.

Chen, C., Zhou, Z., Ross, J.S., Zhou, W., Dong, J.T., 2007. The amplified WWP1 gene is a potential molecular target in breast cancer. Int. J. Cancer 121, 80–87.

Chen, D., Shan, J., Zhu, W.G., Qin, J., Gu, W., 2010. Transcription-independent ARF regulation in oncogenic stress-mediated p53 responses. Nature 464, 624–627.

Chen, D.L., Kon, N., Li, M.Y., Zhang, W.Z., Qin, J., Gu, W., 2005. ARF-BP1/mule is a critical mediator of the ARF tumor suppressor. Cell 121, 1071–1083.

Ciechanover, A., Finley, D., Varshavsky, A., 1984. The ubiquitin-mediated proteolytic pathway and mechanisms of energy-dependent intracellular protein degradation. J. Cell Biochem. 24, 27–53.

Collins 3rd, J.J., Hou, X., Romanova, E.V., Lambrus, B.G., Miller, C.M., Saberi, A., Sweedler, J.V., Newmark, P.A., 2010. Genome-wide analyses reveal a role for peptide hormones in planarian germline development. PLoS Biol. 8, e1000509.

Cowles, M.W., Brown, D.D., Nisperos, S.V., Stanley, B.N., Pearson, B.J., Zayas, R.M., 2013. Genome-wide analysis of the bHLH gene family in planarians identifies factors required for adult neurogenesis and neuronal regeneration. Development 140, 4691–4702.

Cowles, M.W., Hubert, A., Zayas, R.M., 2012. A Lissencephaly-1 homologue is essential for mitotic progression in the planarian *Schmidtea mediterranea*. Dev. Dyn. 241, 901–910.

Cowles, M.W., Omuro, K.C., Stanley, B.N., Quintanilla, C.G., Zayas, R.M., 2014. COE loss-of-function analysis reveals a genetic program underlying maintenance and regeneration of the nervous system in planarians. PLoS Genet. 10, e1004746.

D'Arca, D., Zhao, X., Xu, W., Ramirez-Martinez, N.C., Lavarone, A., Lasorella, A., 2010. Huwe1 ubiquitin ligase is essential to synchronize neuronal and glial differentiation in the developing cerebellum. Proc. Natl. Acad. Sci. USA 107, 5875–5880.

Eisenhoffer, G.T., Kang, H., Sánchez Alvarado, A., 2008. Molecular analysis of stem cells and their descendants during cell turnover and regeneration in the planarian *Schmidtea mediterranea*. Cell Stem Cell 3, 327–339.

Férnandez-Taboada, E., Rodríguez-Esteban, G., Saló, E., Abril, J.F., 2011. A proteomics approach to decipher the molecular nature of planarian stem cells. BMC Genomics 12, 133.

Forsthoefel, D.J., James, N.P., Escobar, D.J., Stary, J.M., Vieira, A.P., Waters, F.A., Newmark, P.A., 2012. An RNAi screen reveals intestinal regulators of branching morphogenesis, differentiation, and stem cell proliferation in planarians. Dev. Cell 23, 691–704.

Forsthoefel, D.J., Newmark, P.A., 2009. Emerging patterns in planarian regeneration. Curr. Opin. Genet. Dev. 19, 412–420.

Forsthoefel, D.J., Park, A.E., Newmark, P.A., 2011. Stem cell-based growth, regeneration, and remodeling of the planarian intestine. Dev. Biol. 356, 445–459.

Gudjonsson, T., Altmeyer, M., Savic, V., Toledo, L., Dinant, C., Grofte, M., Bartkova, J., Poulsen, M., Oka, Y., Bekker-Jensen, S., Mailand, N., Neumann, B., Heriche, J.K., Shearer, R., Saunders, D., Bartek, J., Lukas, J., Lukas, C., 2012. TRIP12 and UBR5 suppress spreading of chromatin ubiquitylation at damaged chromosomes. Cell 150, 697–709.

Gurley, K.A., Rink, J.C., Sánchez Alvarado, A., 2008. Beta-catenin defines head versus tail identity during planarian regeneration and homeostasis. Science 319, 323–327.

Hendzel, M.J., Wei, Y., Mancini, M.A., VanHooser, A., Ranalli, T., Brinkley, B.R., BazettJones, D.P., Allis, C.D., 1997. Mitosis-specific phosphorylation of histone H3 initiates primarily within pericentromeric heterochromatin during G2 and spreads in an ordered fashion coincident with mitotic chromosome condensation. Chromosoma 106, 348–360.

Hershko, A., Ciechanover, A., 1998. The ubiquitin system. Annu. Rev. Biochem. 67, 425–479.

Hubert, A., Henderson, J.M., Ross, K.G., Cowles, M.W., Torres, J., Zayas, R.M., 2013. Epigenetic regulation of planarian stem cells by the SET1/MLL family of histone methyltransferases. Epigenetics 8, 79–91.

Huibregtse, J.M., Scheffner, M., Beaudenon, S., Howley, P.M., 1995. A family of proteins structurally and functionally related to the E6-AP ubiquitin–protein ligase. Proc. Natl. Acad. Sci. USA 92, 2563–2567.

Inoue, S., Hao, Z.Y., Elia, A.J., Cescon, D., Zhou, L., Silvester, J., Snow, B., Harris, I.S., Sasaki, M., Li, W.Y., Itsumi, M., Yamamoto, K., Ueda, T., Dominguez-Brauer, C., Gorrini, C., Chio, I.I.C., Haight, J., You-Ten, A., McCracken, S., Wakeham, A., Ghazarian, D., Penn, L.J.Z., Melino, G., Mak, T.W., 2013. Mule/Huwe1/Arf-BP1 suppresses ras-driven tumorigenesis by preventing c-Myc/Miz1-mediated down-regulation of p21 and p15. Genes Dev. 27, 1101–1114.

Jacobson, A.D., Zhang, N.Y., Xu, P., Han, K.J., Noone, S., Peng, J.M., Liu, C.W., 2009. The lysine 48 and lysine 63 ubiquitin conjugates are processed differently by the 26S proteasome. J. Biol. Chem. 284, 35485–35494.

King, R.S., Newmark, P.A., 2013. In situ hybridization protocol for enhanced detection of gene expression in the planarian *Schmidtea mediterranea*. BMC Dev. Biol. 13, 8.

Kipreos, E.T., 2005. Ubiquitin-mediated pathways in *C. elegans*. WormBook, 2007/12/01, pp. 1–24.

Komander, D., 2009. The emerging complexity of protein ubiquitination. Biochem. Soc. Trans. 37, 937–953.

Labbé, R.M., Irimia, M., Currie, K.W., Lin, A., Zhu, S.J., Brown, D.D.R., Ross, E.J., Voisin, V., Bader, G.D., Blencowe, B.J., Pearson, B.J., 2012. A comparative transcriptomic analysis reveals conserved features of stem cell pluripotency in planarians and mammals. Stem Cells 30, 1734–1745.

Larkin, M.A., Blackshields, G., Brown, N.P., Chenna, R., McGettigan, P.A., McWilliam, H., Valentin, F., Wallace, I.M., Wilm, A., Lopez, R., Thompson, J.D., Gibson, T.J., Higgins, D.G., 2007. Clustal W and clustal X version 2.0. Bioinformatics 23, 2947–2948.

Lauter, G., Soll, I., Hauptmann, G., 2011. Two-color fluorescent in situ hybridization in the embryonic zebrafish brain using differential detection systems. BMC Dev. Biol. 11, 43.

Marín, I., 2010. Animal HECT ubiquitin ligases: evolution and functional implications. BMC Evol. Biol. 10, 56.

Marín, I., 2013. Evolution of plant HECT ubiquitin ligases. PLoS One 8, e68536.

Metzger, M.B., Hristova, V.A., Weissman, A.M., 2012. HECT and RING finger families of E3 ubiquitin ligases at a glance. J. Cell Sci. 125, 531–537.

Newmark, P.A., Sánchez Alvarado, A., 2002. Not your father's planarian: a classic model enters the era of functional genomics. Nat. Rev. Genet. 3, 210–219.

Newmark, P.A., Wang, Y., Chong, T., 2008. Germ cell specification and regeneration in planarians. Cold Spring Harb. Symp. Quant. Biol. 73, 573–581.

Nicholas, K., Nicholas, H.j., 1997. GeneDoc: a tool for editing and annotating multiple sequence alignments. Distributed by the author.

Önal, P., Grün, D., Adamidi, C., Rybak, A., Solana, J., Mastrobuoni, G., Wang, Y., Rahn, H.-P., Chen, W., Kempa, S., Ziebold, U., Rajewsky, N., 2012. Gene expression of pluripotency determinants is conserved between mammalian and planarian stem cells. EMBO J. 31, 2755–2769.

Oviedo, N.J., Levin, M., 2007. smedinx-11 is a planarian stem cell gap junction gene required for regeneration and homeostasis. Development 134, 3121–3131.

Oviedo, N.J., Pearson, B.J., Levin, M., Sánchez Alvarado, A., 2008. Planarian PTEN homologs regulate stem cells and regeneration through TOR signaling. Dis. Model. Mech. 1, 131–143 (discussion 141).

Pearson, B.J., Eisenhoffer, G.T., Gurley, K.A., Rink, J.C., Miller, D.E., Sánchez Alvarado, A., 2009. Formaldehyde-based whole-mount in situ hybridization method for planarians. Dev. Dyn. 238, 443–450.

Pearson, B.J., Sánchez Alvarado, A., 2008. Regeneration, stem cells, and the evolution of tumor suppression. Cold Spring Harb. Symp. Quant. Biol. 73, 565–572.

Pearson, B.J., Sánchez Alvarado, A., 2010. A planarian p53 homolog regulates proliferation and self-renewal in adult stem cell lineages. Development 137, 213–221.

Pellettieri, J., Fitzgerald, P., Watanabe, S., Mancuso, J., Green, D.R., Sánchez Alvarado, A., 2010. Cell death and tissue remodeling in planarian regeneration. Dev. Biol. 338, 76–85.

Petersen, C.P., Reddien, P.W., 2009. A wound-induced Wnt expression program controls planarian regeneration polarity. Proc. Natl. Acad. Sci. USA 106, 17061–17066.

Pomerantz, J.H., Blau, H.M., 2013. Tumor suppressors: enhancers or suppressors of regeneration? Development 140, 2502–2512.

Qi, C.F., Kim, Y.S., Xiang, S., Abdullaev, Z., Torrey, T.A., Janz, S., Kovalchuk, A.L., Sun, J., Chen, D., Cho, W.C., Gu, W., Morse 3rd, H.C., 2012. Characterization of ARF-BP1/HUWE1 interactions with CTCF, MYC, ARF and p53 in MYC-driven B cell neoplasms. Int. J. Mol. Sci. 13, 6204–6219.

Reddien, P.W., 2011. Constitutive gene expression and the specification of tissue identity in adult planarian biology. Trends Genet. 27, 277–285.

Reddien, P.W., Bermange, A.L., Murfitt, K.J., Jennings, J.R., Sánchez Alvarado, A., 2005. Identification of genes needed for regeneration, stem cell function, and tissue homeostasis by systematic gene perturbation in planaria. Dev. Cell 8, 635–649.

Reddien, P.W., Sánchez Alvarado, A., 2004. Fundamentals of planarian regeneration. Annu. Rev. Cell Dev. Biol. 20, 725–757.

Resch, A.M., Palakodeti, D., Lu, Y.C., Horowitz, M., Graveley, B.R., 2012. Transcriptome analysis reveals strain-specific and conserved stemness genes in *Schmidtea mediterranea*. PLoS One 7, e34447.
Romero, B.T., Evans, D.J., Aboobaker, A.A., 2012. FACS analysis of the planarian stem cell compartment as a tool to understand regenerative mechanisms. Methods Mol. Biol. 916, 167–179.
Rotin, D., Kumar, S., 2009. Physiological functions of the HECT family of ubiquitin ligases. Nat. Rev. Mol. Cell Biol. 10, 398–409.
Sánchez Alvarado, A., 2004. Planarians. Curr. Biol. 14, R737–R738.
Sánchez Alvarado, A., 2007. Stem cells and the planarian *Schmidtea mediterranea*. C. R. Biol. 330, 498–503.
Sánchez Alvarado, A., Newmark, P.A., 1999. Double-stranded RNA specifically disrupts gene expression during planarian regeneration. Proc. Natl. Acad. Sci. USA 96, 5049–5054.
Sarkar, A., Hochedlinger, K., 2013. The sox family of transcription factors: versatile regulators of stem and progenitor cell fate. Cell Stem Cell 12, 15–30.
Scheffner, M., Nuber, U., Huibregtse, J.M., 1995. Protein ubiquitination involving an E1–E2–E3 enzyme ubiquitin thioester cascade. Nature 373, 81–83.
Scheffner, M., Staub, O., 2007. HECT E3s and human disease. BMC Biochem. 8 (Suppl. 1), S6.
Schneider, C.A., Rasband, W.S., Eliceiri, K.W., 2012. NIH image to imageJ: 25 years of image analysis. Nat. Methods 9, 671–675.
Subik, K., Shu, L., Wu, C.Y., Liang, Q.Q., Hicks, D., Boyce, B., Schiffhauer, L., Chen, D., Chen, C.S., Tang, P., Xing, L.P., 2012. The ubiquitin E3 ligase WWP1 decreases CXCL12-mediated MDA231 breast cancer cell migration and bone metastasis. Bone 50, 813–823.
Swofford, D., 2003. PAUP*: Phylogenetic Analysis Using Parsimony (*and Other Methods). Version 4. Sinauer Associates, Sunderland, Massachusetts.
Tamura, K., Peterson, D., Peterson, N., Stecher, G., Nei, M., Kumar, S., 2011. MEGA5: molecular evolutionary genetics analysis using maximum likelihood, evolutionary distance, and maximum parsimony methods. Mol. Biol. Evol. 28, 2731–2739.
van Wolfswinkel, J.C., Wagner, D.E., Reddien, P.W., 2014. Single-cell analysis reveals functionally distinct classes within the planarian stem cell compartment. Cell Stem Cell 15, 326–339.
Wang, X., Lu, G., Li, L., Yi, J., Yan, K., Wang, Y., Zhu, B., Kuang, J., Lin, M., Zhang, S., Shao, G., 2014. HUWE1 interacts with BRCA1 and promotes its degradation in the ubiquitin–proteasome pathway. Biochem. Biophys. Res. Commun. 444, 290–295.
Wang, Y., Stary, J.M., Wilhelm, J.E., Newmark, P.A., 2010. A functional genomic screen in planarians identifies novel regulators of germ cell development. Genes Dev. 24, 2081–2092.
Wenemoser, D., Lapan, S.W., Wilkinson, A.W., Bell, G.W., Reddien, P.W., 2012. A molecular wound response program associated with regeneration initiation in planarians. Genes Dev. 26, 988–1002.
Yazawa, S., Umesono, Y., Hayashi, T., Tarui, H., Agata, K., 2009. Planarian Hedgehog/Patched establishes anterior–posterior polarity by regulating Wnt signaling. Proc. Natl. Acad. Sci. USA 106, 22329–22334.
Zayas, R.M., Hernández, A., Habermann, B., Wang, Y., Stary, J.M., Newmark, P.A., 2005. The planarian *Schmidtea mediterranea* as a model for epigenetic germ cell specification: analysis of ESTs from the hermaphroditic strain. Proc. Natl. Acad. Sci. USA 102, 18491–18496.
Zhi, X., Chen, C.S., 2012. WWP1: a versatile ubiquitin E3 ligase in signaling and diseases. Cell. Mol. Life Sci. 69, 1425–1434.